Int. J. Heat Mass Transfer. Vol. 26, No. 1, pp. 33–40, 1983
Printed in Great Britain

0017–9310/83/010033–08 $03.00/0

HEAT TRANSFER AT AN ARRAY OF CO-PLANAR SLAT-LIKE SURFACES ORIENTED NORMAL TO A FORCED CONVECTION FLOW

E. M. SPARROW, W. Q. TAO and D. D. RADTKE
Department of Mechanical Engineering, University of Minnesota, Minneapolis, MN 55455, U.S.A.

(*Received* 23 *February* 1981 *and in final form* 21 *May* 1982)

Abstract—Measurements of the per-slat heat transfer coefficient were made for an array of co-planar slat-like surfaces which face upstream into an oncoming flow. The flow washes over the slats as it passes into slot-like gaps between the slats. The experiments were performed for four different slat–slot configurations characterized by the ratio of the slot width to the slat width, and the slot Reynolds number was varied by more than an order of magnitude. Auxiliary experiments encompassing flow visualization and variations of the number of slots were carried out to demonstrate that the results are not influenced by end effects and by the finite number of slots employed. It was found that the dependence of the Nusselt number on the Reynolds number was the same for all of the array configurations investigated and that the influence of the array geometry was very well represented by a power law. This led to the global correlation $Nu_P = 1.19\,Re^{0.465}\,Pr^{0.375}\,(P/W)^{1.4}$ from which the RMS deviation of the data was only 1.1%.

NOMENCLATURE

- C, constant in Sh, Re relation;
- D_h, hydraulic diameter, equation (4);
- $\mathscr{D}$, diffusion coefficient;
- H, slot width;
- h, per-slat heat transfer coefficient;
- K, per-slat mass transfer coefficent;
- k, thermal conductivity;
- L, transverse length of slat-slot array;
- $\dot{m}$, mass transfer rate per unit area;
- N, number of slots;
- Nu_P, per-slat Nusselt number, hP/K;
- n, exponent in Sh, Re relation;
- P, pitch, $(W + H)$;
- Pr, Prandtl number;
- Re, slot Reynolds number, $\rho V D_h/\mu$;
- Sc, Schmidt number;
- Sh_P, per-slat Sherwood number, $KP/\mathscr{D}$;
- V, mean velocity in slot;
- W, slat width;
- $\dot{w}$, rate of mass flow through array.

Greek symbols

- μ, viscosity of flowing fluid;
- ν, kinematic viscosity of flowing fluid;
- ρ, density of flowing fluid;
- ρ_{nw}, density of naphthalene vapor at surface;
- $\rho_{n\infty}$, density of naphthalene vapor in approach flow.

INTRODUCTION

THIS paper is concerned with the heat transfer characteristics of an array of co-planar slat-like surfaces which face upstream into an oncoming airflow. The flow washes over the slats as it passes from the upstream space into the slot-like gaps between the slats. A schematic diagram depicting the physical situation is presented in Fig. 1, which is a head-on view looking toward the slat-slot array from an upstream vantage point. The direction of the flow approaching the array is perpendicular to the plane of the figure.

One among the various physical situations that are modeled by the aforementioned slat-slot array is that encountered at the inlet of a stacked, channel-type heat exchanger. Such a heat exchanger consists of two sets of high-aspect-ratio rectangular channels, with the channels of one set being interleaved between the channels of the other set. Typically the fluid flows in the two sets of channels are at right angles. The fluid entering one set of channels sees an array of slots (the inlets of the respective channels) which alternate with an array of solid slat-like surfaces (the side walls of the second set of channels). In the course of its flow into the slots, the fluid washes over the slats, and convective heat transfer will occur. Other applications involving slat-slot arrays include ribbon-type parachutes and grilles, vents, and grates.

The focus of the research is the experimental determination of the per-slat heat transfer coefficient as a function of both fluid flow and geometrical parameters. As shown in Fig. 1, the slat-slot configuration is fixed by the slat width W and slot width H or, alternatively, by the pitch $P\,(= W + H)$ and either H or W. In dimensionless terms, the configuration may be specified by the ratio H/W, and the apparatus was varied during the course of the experiments to provide four values of H/W in the range from 0.4 to 1.5.

Another geometry-related issue that was investigated during the research was the possible effects of the finiteness of the array (i.e. end effects) on the measured heat transfer coefficients. In this connection, the number of slat-slot pairs was varied, and the data for the different numbers of pairs were compared. Furthermore, to avoid end effects associated with the finiteness

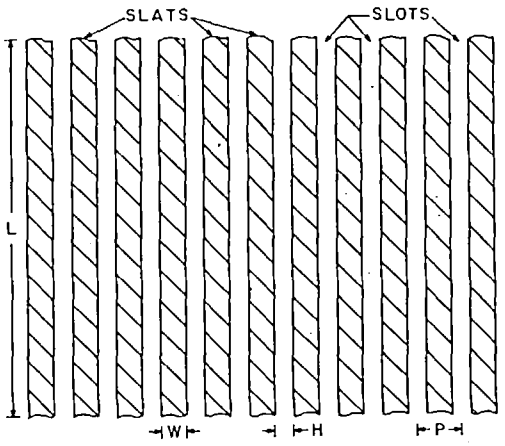

FIG. 1. Head-on view of a slat-slot array looking from an upstream vantage point.

of the slat-slot length L (see Fig. 1), data were collected only in the central region of the length, i.e. away from the ends. Supplementary flow visualization experiments were performed to verify the absence of end effects in the measurement region. The oil–lampblack technique was used for the visualization work.

The Reynolds number used to characterize the fluid flow was defined on the basis of the mean velocity in the slots and the slot hydraulic diameter. The range of the Reynolds number extended from 500 to 7000, which spans the conditions commonly encountered in compact heat exchangers.

In the presentation of results, it was found possible to obtain a virtually perfect correlation for the Nusselt number as a function of both Re and P/W. The excellence of the correlation suggests that the correlating equation can be safely used for extrapolations to Re and P/W values outside the range investigated here.

A survey of the literature did not disclose any experimental or theoretical information which could be compared to the data obtained here. Among the candidates considered for comparison was the classical problem of plane stagnation flow, whereby a uniform stream impinges normal to a flat plate. In that case, however, there is nothing in the flow pattern that corresponds to the turning experienced by the fluid which passes over a slat and enters the adjacent slot.

THE EXPERIMENTS

The attainment of the objectives described in the Introduction was facilitated by the use of the naphthalene sublimation technique in lieu of direct heat transfer measurements. Had heat transfer experiments been made, it would not have been possible to determine the transfer coefficients at the upstream-facing surface of the slat with the desired accuracy. In any realistic heat transfer setup, conduction within the slat would operate to create thermal interactions between the upstream face of the slat, its lateral edges (i.e. the edges which form the walls of the slot), and its downstream face. In addition, conduction would act to create end-effect problems. As a consequence of these characteristics, there would be uncertainties in the rate of heat transfer at the upstream surface and in the thermal boundary condition at that surface. These difficulties do not exist with the naphthalene technique where, in fact, the rate of mass transfer can be determined to better than 1% and a boundary condition analogous to uniform wall temperature is readily attained.

In view of the analogy between heat and mass transfer [1], the mass transfer coefficients determined here can be readily transformed to heat transfer coefficients. Consequently, the phrases heat transfer and mass transfer will be used interchangeably throughout the presentation of results. The transformation of the dimensionless mass transfer coefficients (Sherwood numbers) into Nusselt numbers will be carried out at the end of the paper.

Experimental apparatus

An overall pictorial diagram of the experimental apparatus is presented in Fig. 2. As seen there, the upper wall of a large chamber serves as the host surface for the slat-slot array. The apparatus is operated in the suction mode, with air from the temperature-controlled laboratory room being drawn through the slots into the chamber. After traversing the height of the chamber, the air exits at the base and is ducted to an air-handling system consisting of flowmeters (calibrated rotameters), control valves, and blowers. The blowers are situated in a service corridor adjacent to the laboratory, and the naphthalene-laden discharge from the blowers is vented outside of the building.

The upper wall of the chamber is a square plate, 68.6 cm on a side, and the height of the chamber is 130 cm. A 17.8 × 38.1 cm rectangular opening was machined into the upper wall in order to accommodate the slotted test section plate shown in Fig. 2. The edges of the opening were fitted with a lap to support and position the plate, and positive sealing against leaks was accomplished by an O-ring which was compressed when screws were tightened on the underside of the lap. During the assembly of the apparatus, the narrow gap between the test section plate and the upper wall of the chamber was filled with body putty, whereafter the entire surface was subjected to a succession of hand sanding and lapping operations. The result was a continuous, mirror-like surface.

During the course of the experiments, four different test plate configurations were employed. A plan view of a typical test section plate is shown in Fig. 3, and the dimensions of the slats and slots for the various configurations are listed in Table 1. As seen in the table, the H/W ratio, which compares the slot width to slat width, ranged from 0.40 to 1.5 (actually 1.49). Correspondingly, the ratio of pitch to slat width, P/W, ranged from 1.40 to 2.5. In addition to the aforementioned ratios and the actual W, H, and L dimensions, the table also lists the hydraulic diameter D_h of the individual slots which will be employed later in the

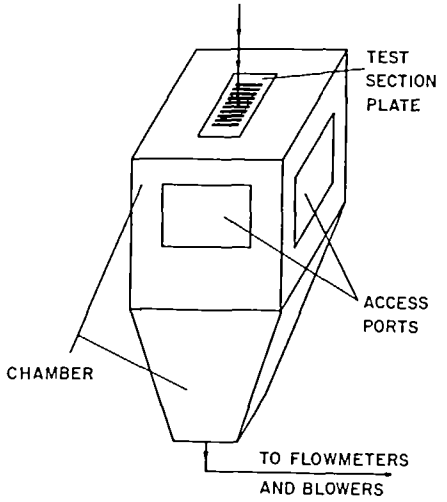

FIG. 2. Overall pictorial view of the experimental apparatus.

evaluation of the Reynolds number. All test plates were milled from 0.635 cm thick aluminum stock.

The slot length L was maintained constant throughout the experiments, and the slot aspect ratio L/H ranged from 8.3 to 25. Flow visualization studies, to be described later, affirmed that even for the smallest aspect ratio, the fluid flow which washed over the mass transfer section was 2-dim., i.e. uninfluenced by the end effects which occur at the extremities of the slot.

The primary experiments were performed with a ten-slot array, as illustrated in Fig. 3. Auxiliary experiments were also performed with an eight-slot array which was obtained from the ten-slot array by closing one slot at each end of the array with pressure-sensitive tape.

Owing to the nature of the fluid flow which passes over the slats, there are no mass transfer interactions between the individual slats. Therefore, experimental results obtained with only one mass-transfer-active slat will apply equally well to the case in which all slats participate in the transfer process. Consequently, as shown in Fig. 3, the experiments were conducted with mass transfer at only one of the slats, the centermost one in the array. This slat will be designated as the test section slat. Individual test section slats were tailored

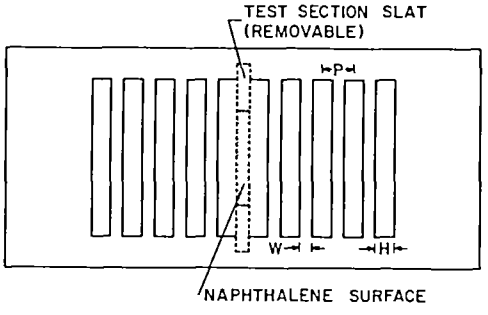

FIG. 3. Plan view of a typical test section plate.

Table 1. Geometrical characteristics of the test section plates (all dimensions in cm)

	Plate no. I	II	III	IV
H/W	0.40	0.75	1.00	1.49
P/W	1.40	1.75	2.00	2.49
H	0.505	0.762	1.267	1.520
W	1.273	1.016	1.273	1.020
P	1.778	1.778	2.540	2.540
L	12.697	12.697	12.675	12.677
D_h	0.971	1.438	2.304	2.715

to the various arrays described in Table 1 by being machined from 0.635 cm thick aluminum plate stock.

Figure 3 indicates the test section slat to be removable from the remainder of the slat-slot array. This feature was incorporated into the design to facilitate both the preparation of a fresh naphthalene surface for each data run and the determination of the sublimed mass — all without having to remove and subsequently replace the entire slat-slot array.

As seen in the figure, the naphthalene portion of the test section slat spanned only 7.26 cm of the 12.7 cm length L of the slat–slot array. This arrangement ensured that the mass transfer occurred in a 2-dim. flow and was free of end effects.

Naphthalene test surfaces

Each test section slat contained a rectangular cavity which was filled with naphthalene by means of a casting procedure. The mold cavity was about 0.38 cm deep and, as noted earlier, spanned 7.62 cm along the slat length. Along its lateral edges (i.e. adjacent to the slot), the cavity was bounded by 0.025 cm thick walls — the thinnest possible walls that could be machined consistent with structural integrity. Thus, the width of the naphthalene section was very slightly less than the overall width W of the slat.

To facilitate the casting procedure, five circular apertures were drilled into the cavity from the rear. One of these, the largest one, was used for pouring molten naphthalene into the mold cavity, while the other four served as air escape vents during the pouring process.

As a first step in the casting process, the naphthalene remaining in the mold cavity from the prior data run was removed by melting and evaporation. Then, the slat was placed on a hand-lapped stainless steel plate such that the open part of the mold cavity faced downward. A funnel was then inserted into the pouring aperture along with risers in the vent holes. After the pouring of the molten naphthalene and its subsequent solidification, the slat was readily separated from the stainless steel casting plate. The finish of the thus-exposed naphthalene surface is believed comparable in quality to that of the hand-lapped plate. Extraneous naphthalene particles and dust were carefully removed from the slat, after which it was wrapped in impermeable plastic and placed in the laboratory.

Instrumentation and experimental procedure

The key instrument used in the experiments was a Sartorius ultra-precise electronic balance capable of being read to 10^{-5} g and having a capacity of 160 g. An ASTM-certified thermometer with a smallest scale division of 0.1°F was used to measure the temperature of the air approaching the slat-slot array. As noted earlier, calibrated rotameters served for the volume-flow determination, while requisite pressure measurements were made with a manometer and a barometer.

Attention will now be turned to the experimental procedure. To prepare for a data run, the test section slat was implanted in the slotted plate situated atop the suction chamber, and a tightly fitting Plexiglas cover was placed over the slat to prevent sublimation. The airflow, set at the desired flowrate, was then initiated, thereby beginning the equilibration period during which the naphthalene test surface was allowed to attain thermal equilibrium with the air passing from the laboratory into the chamber. The duration of the equilibration period ranged from 1 to 3 h, depending on the Reynolds number.

Immediately before the intended start of the data run, the test section slat was removed from the slotted plate and weighed (with the cover removed). Upon completion of the weighing, the cover was replaced and the slat and cover were reinstalled in the slotted plate. The slat was then fixed in place and the slotted plate sealed against leaks by tightening screws at the rear of the lap on which the plate rested. This was accomplished via one of the access ports on the side of the suction chamber (Fig. 2), after which the port was sealed. At this point, the Plexiglas cover was removed from the test section slat and timing was initiated, thereby marking the start of the data run.

The duration of the run was selected to limit the average recession of the naphthalene surface to less than 0.0025 cm. This criterion yielded run times between 30 and 120 min, depending on the Reynolds number and the geometrical parameters. During the run, temperature, flow rate, and pressure data were collected periodically. At the preselected termination of the run, the Plexiglas cover was placed atop the test section slat and the blowers deactivated. The slat was then weighed (with the cover removed).

To affirm that there were no extraneous losses in the period between the first and second weighings, a so-called after-run was performed following each data run. In this procedure, all of the steps subsequent to the first weighing were repeated, with the exception of the exposure of the naphthalene surface to the airflow. The change of mass for the after-run was typically 0.05 mg, which is only about 0.2% of the mass sublimed during the data run proper.

Flow visualization

The oil-lampblack technique was used as the visualization tool. Lampblack, a very fine black powder, is mixed with an oil, and the mixture is brushed on the surface whose fluid flow characteristics are to be studied. Under the action of shear stresses exerted by the flow, an array of streaks is formed on the surface as the oil–lampback mixture follows the path of the fluid particles that pass adjacent to the surface.

The sharpness of the visualization pattern depends on the fluidity of the mixture as well as on the magnitude of the shear stresses. To facilitate the visualization, a number of oils of different viscosities were assembled and various trial mixtures were formulated and employed in preliminary runs. For all visualization runs, both preliminary and final, the slats were covered with a white, plasticized, self-adhering contact paper in order to provide the highest possible contrast for the streak lines. A typical streak line pattern will be presented later.

Data reduction

To begin the data reduction, the measured change of mass during the data run (corrected in accordance with the after-run) is divided by the duration of the run and by the mass transfer surface area, yielding the mass flux $\dot{m}$. When, in turn, $\dot{m}$ is divided by the density difference $(\rho_{nw} - \rho_{n\infty})$ which drives the mass transfer, the mass transfer coefficient follows as

$$K = \dot{m}/(\rho_{nw} - \rho_{n\infty}). \quad (1)$$

The quantity ρ_{nw} is the density of the naphthalene vapor that is in equilibrium with the solid naphthalene surface in the test section slat, while $\rho_{n\infty}$ is the naphthalene vapor density in the flow approaching the slotted plate.

In the present experiments, $\rho_{n\infty}$ is zero. To determine ρ_{nw}, a naphthalene vapor pressure–temperature relation (e.g. the Sogin equation [2]) can be used in conjunction with the perfect gas law and with the temperature of the solid naphthalene surface. In view of the lengthy equilibration period that preceded each data run, the only possible causes of deviation between the measured air temperature and the naphthalene surface temperature are: (a) differences between the stagnation temperature of the air and the recovery temperature of the surface and (b) a temperature depression of the surface which induces heat transfer from the air to the surface to supply the required latent heat of sublimation. With regard to the first of these, it was shown by calculation to be entirely negligible ($\ll 0.01$°C). For the temperature depression, an extreme value of 0.08°C was calculated, which corresponds to an uncertainty in ρ_{nw} of about 0.8%. This uncertainty, the largest in the entire experiment, is fully tolerable.

The dimensionless counterpart of the mass transfer coefficient is the Sherwood number (analogous to the Nusselt number). In defining the Sherwood number, it is necessary to specify a characteristic dimension and, *a priori*, there is no definitive reason for selecting one among the several that may be considered (i.e. H, W, P and D_h). However, in the final correlation of the results, it was found that a Sherwood number based on the pitch P served very well. Therefore, on that basis,

$$Sh_P = KP/\mathscr{D}. \quad (2)$$

Furthermore, since the diffusion coefficient $\mathscr{D} = \nu/Sc$ (Sc = Schmidt number), equation (2) becomes

$$Sh_P = (KP/\nu)Sc \quad (3)$$

in which ν is the kinematic viscosity of air. The value of Sc for naphthalene diffusion in air is 2.5 [2].

The other dimensionless group that is relevant to the problem is the Reynolds number. For the Reynolds number, as for the Sherwood number, there is some freedom of definition. In this regard, it is believed that the slot Reynolds number, based on the slot hydraulic diameter D_h and mean velocity V, will have more physical meaning to practitioners and researchers than other alternatives. If it is noted that the per-slot cross-sectional area and perimeter are respectively equal to LH and $2(L + H)$, then

$$\rho V = \dot{w}/NLH, \quad D_h = 2LH/(L + H) \quad (4)$$

and

$$Re = \rho V D_h/\mu = 2\dot{w}/N\mu(L + H) \quad (5)$$

where $\dot{w}$ is the mass flow through the array of slots and N is the number of slots.

As indicated in equation (5), the total mass flow has been prorated uniformly among the slots. The prorating will be revisited when results for different numbers of slots are presented.

RESULTS AND DISCUSSION

The presentation of results will begin with the Sherwood number data for each of the individual arrays and then goes on to a global Sherwood number correlation which encompasses all of the array geometries and Reynolds numbers investigated here. Attention is next turned to the transformation of the mass transfer results into heat transfer results. The flow visualization results will conclude the presentation.

Mass transfer results

The slat Sherwood numbers for the individual arrays are plotted as a function of the Reynolds number in Figs. 4–7. The successive figures correspond to ratios of slot width to slat width H/W equal to 0.40, 0.75, 1.0 and 1.49. Overall, the Reynolds number spans the range from 500 to 7000, which encompasses the operating conditions encountered in stacked channel-type compact heat exchangers (see Introduction).

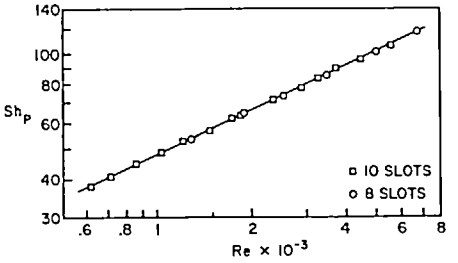

FIG. 5. Slat Sherwood numbers for a slat-slot array with a ratio of slot width to slat width $H/W = 0.75$.

In each figure, data are presented for both 10-slot and 8-slot arrays (square and circle data symbols, respectively). The primary experiments were performed for the 10-slot array, and the 8-slot array served as a supplementary case that was investigated to corroborate that the results were not affected by the finite number of slots. Correspondingly, fewer data were collected for the 8-slot array.

In addition to the experimental data, each figure contains a least-squares straight line which represents the power law

$$Sh_P = CRe^n. \quad (6)$$

The constants C and n for the various arrays are listed in Table 2.

Inspection of Figs. 4–7 indicates characteristics that are common to all of the investigated arrays. First of all, the Sherwood number increases monotonically and regularly with the Reynolds number, and it is clear that the power-law relation (6) is a proper representation of the dependence of Sh_P on Re. It is especially noteworthy (from Table 2) that the Reynolds number exponents n for the various arrays lie in such a narrow range, 0.461–0.471, that it is improbable that the variation of n with H/W is physically significant. Thus, a common value such as $n = 0.465$ (the average of the n values of Table 2) can be employed for all the arrays, as will be demonstrated shortly.

It is relevant to observe that the aforementioned n value of 0.465 is very close to the value 0.476 which appears in a power-law correlation for the heat (mass) transfer coefficient for the upstream face of a plate perforated with circular holes [3]. Furthermore, it

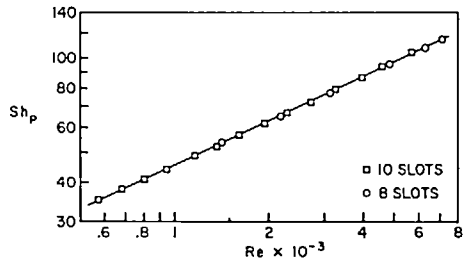

FIG. 4. Slat Sherwood numbers for a slat-slot array with a ratio of slot width to slat width $H/W = 0.40$.

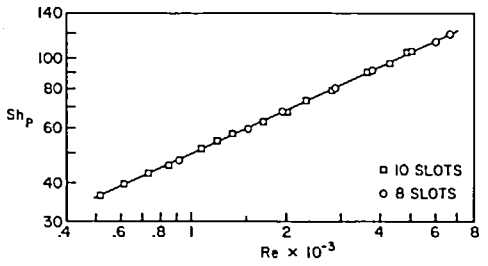

FIG. 6. Slat Sherwood numbers for a slat-slot array with a ratio of slot width to slat width $H/W = 1.00$.

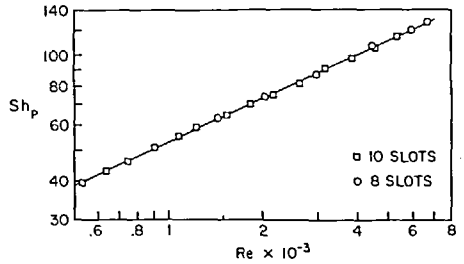

FIG. 7. Slat Sherwood numbers for a slat-slot array with a ratio of slot width to slat width $H/W = 1.49$.

Table 2. Values of C and n for equation (6)

H/W	C	n
0.40	1.75	0.471
0.75	1.91	0.466
1.00	2.03	0.462
1.49	2.19	0.461

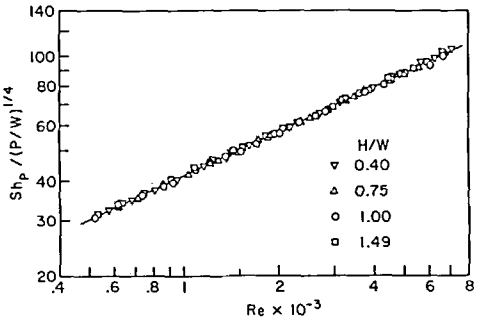

FIG. 8. Global correlation of the slat Sherwood numbers for all of the investigated arrays and Reynolds numbers.

differs only slightly from the value 0.5 which characterizes laminar stagnation flows. The present flow field has certain features in common with the classical plane stagnation flow. However, as noted earlier, the turning of the flow as it enters the slot is a feature not found in the classical case.

Another important result in evidence in Figs. 4–7 is the complete agreement, within the slight scatter of the data, of the Sherwood numbers for the 8- and 10- slot arrays. This finding has particular significance with regard to the uniform prorating of the mass flow among the various slots that was assumed in the data reduction procedure. If, in the actual experiments, there had been significant departures from uniform prorating, this would be reflected by deviations between the data for different numbers of slots. The absence of such deviations supports the assertion that the results obtained here are not influenced by the finite number of slots.

As a final observation in connection with Figs. 4–7, note may be taken of minimal scatter in the data. Typically, the data scatter is about 2% relative to the respective correlating lines.

Attention may now be turned to the formulation of a global correlation of the results for all the investigated arrays. The initial efforts were directed towards finding an equation of the form $Sh = C' Re^m$ which would describe all the results, where C' is a constant independent of the geometrical parameters. In this correlation effort, the characteristic dimensions that appear in Sh and Re were left open, and various combinations of the lengths H, W, P and D_h were employed in the evaluation of Sh and Re. This procedure did not yield the desired universal correlation of the data.

Efforts were next directed toward implementing a correlation of the form $Sh = C'' Re^m G^q$, where G is a ratio of characteristic lengths (e.g. P/W, H/W) and C'' is a universal constant. These efforts were eminently successful, yielding

$$Sh_P = 1.68 Re^{0.465} (P/W)^{1/4} \tag{7}$$

where Sh_P and Re are defined in equations (3) and (5). The excellence of the global correlation can be assessed by inspection of Fig. 8. In this figure, the data for all the arrays are plotted in the form $Sh_P/(P/W)^{1/4}$ vs Re along with equation (7). Of the 82 data points plotted in the figure, 51 lie within 1% of the correlating line and only one point deviates by more than 3% (actually, 3.3%). The RMS deviation of the data from the line is 1.1%.

The excellence with which equation (7) represents the data, both with respect to variations in Reynolds number and P/W, invites its extrapolation to Re and P/W values beyond those investigated here.

Heat transfer results

The analogy between heat and mass transfer states that at a given Reynolds number, the Sherwood number corresponding to a given Schmidt number is equal to the Nusselt number for a fluid whose Prandtl number is numerically equal to the Schmidt number. Consequently, by making use of equation (7) and recalling that the Schmidt number is equal to 2.5 for

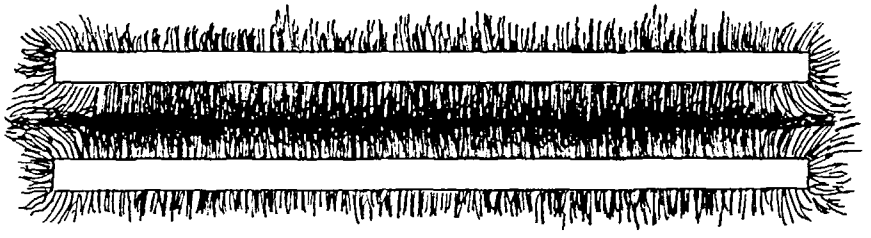

FIG. 9. Portrayal of the pattern of fluid flow adjacent to the surface of a slat.

naphthalene sublimation in air

$$Nu_P = 1.68Re^{0.465}(P/W)^{1.4}, \quad Pr = 2.5. \qquad (8)$$

It remains to generalize equation (8) to Prandtl numbers other than 2.5. In this regard, it is common practice to employ a power-law dependence Pr^s. For external flows, $s = 1/3$ is more or less standard in the older literature, but more recent correlations have used s values of 0.37 [4] and 0.4 [5]. For plane stagnation flow (a case with which the present flow pattern has certain features in common), analytically determined heat transfer coefficients [6] are correlated within 1% or better in the range $0.7 \leqslant Pr \leqslant 10$ with $Pr^{0.375}$. In light of the foregoing information, it appears that $Pr^{0.375}$ provides a reasonable representation of the Prandtl number effect. With this, equation (8) becomes

$$Nu_P = 1.19Re^{0.465}\,Pr^{0.375}\,(P/W)^{1.4}. \qquad (9)$$

Equation (9) represents the most general version of the present results in a form that is applicable to heat transfer applications.

Flow visualization results

A sketch portraying the visual observations from the oil–lampback flow visualization patterns is presented in Fig. 9. Since the flow pattern is periodic, it is only necessary to display a typical module, as in Fig. 9 which shows a slat flanked by two slots. In interpreting the figure, it should be noted that prior to the initiation of the airflow, the slats and the adjacent portion of the test section plate were covered with a uniform black coating (i.e. the oil–lampback mixture). Thus, the pattern in evidence in Fig. 9 represents a significant rearrangement of the oil–lampback mixture in response to the forces exerted by the fluid flow.

The black band which runs the length of the slat is a stagnation line which separates the fluid which streams toward one of the slots from the fluid which streams toward the other slot. A stagnation line appears as a black band because the shear stresses in a stagnation region are too weak to move the oil–lampback mixture. Except near the ends of the slots, the pattern of parallel streaklines which emanate from the stagnation line indicate that the flow is 2-dim. The 3-dim. motions, as revealed by the curving streaklines, are confined to the very near neighborhood of the ends.

The mass transfer section occupied the central two-thirds of the length of a slat. Therefore, in light of Fig. 9, this section was far removed from the hydrodynamic end effects and, correspondingly, the mass transfer was unaffected by the finite length of the slot.

CONCLUDING REMARKS

The experiments performed here have provided definitive heat transfer information for an array of co-planar slat-like surfaces which face upstream into an oncoming flow. The flow washes over the slats as it passes into slot-like gaps between the slats. During the course of the experiments, four different slat-slot configurations were employed — characterized by the ratio of the slot width to the slat width H/W which ranged from 0.4 to 1.5. The slot Reynolds number Re was varied from 500 to 7000, which encompasses the operating conditions encountered in compact heat exchangers.

To obtain results of high accuracy corresponding to a well defined thermal boundary condition, the naphthalene sublimation technique was employed in lieu of direct heat transfer measurements. The dimensionless mass transfer coefficients (i.e. Sherwood numbers) were transformed to Nusselt numbers by means of the analogy between heat and mass transfer.

Auxiliary experiments were performed to demonstrate that the results were not influenced by end effects and by the finite number of slots employed. These supplementary experiments included both flow visualization and variation of the number of slots.

The mass transfer results for all the slat-slot arrays obeyed the power law $Sh_P = CRe^n$ with high fidelity. The n values were virtually the same for all the arrays, averaging to $n = 0.465$, whereas the C's varied with H/W (or, equivalently, with the ratio of the pitch to the slat width P/W). A global correlation of the Sherwood number data, encompassing all of the investigated Reynolds numbers and array parameters, is given by equation (7). The excellence of the correlation is witnessed by the fact that only one data point among the 82 collected fell more than 3% from the correlating line (actually, 3.3%).

The aforementioned global correlation for the Sherwood number was transformed into a Nusselt number correlation, after which a power law was employed to generalize the range of the Prandtl number. The final expression for the Nusselt number is

$$Nu_P = 1.19Re^{0.465}\,Pr^{0.375}\,(P/W)^{1.4}.$$

The high degree of fidelity with which this equation represents the data, both with respect to variations in Reynolds number and P/W, suggests its extrapolation to Re and P/W values beyond those investigated here.

Acknowledgement — The research reported here was performed under the auspices of the National Science Foundation.

REFERENCES

1. E. R. G. Eckert, Analogies to heat transfer processes, in *Measurements in Heat Transfer* (Edited by E. R. G. Eckert and R. J. Goldstein). Hemisphere, Washington, D.C. (1976).
2. H. H. Sogin, Sublimation from disks to airstreams flowing normal to their surfaces, *Trans. ASME* **80**, 61–71 (1958).
3. E. M. Sparrow and M. Carranco Ortiz, Heat transfer coefficients for the upstream face of a perforated plate positioned normal to an oncoming flow, *Int. J. Heat Mass Transfer* **25**, 127–135 (1982).
4. A. A. Zukauskas, Heat transfer from tubes in crossflow, *Adv. Heat Transfer* **8**, 93–160 (1972).

5. S. Whitaker, Forced convection heat transfer correlations for flow in pipes, past flat plates, single cylinders, single spheres, and for flow in packed beds and tube bundles, *A.I.Ch.E. Jl* **18**, 361–365 (1972).
6. E. M. Sparrow and L. Lee, Analysis of flow field and impingement heat/mass transfer due to a nonuniform slot jet, *Trans. Am. Soc. Mech. Engrs*, Series C, *J. Heat Transfer* **97**, 191–197 (1975).

TRANSFERT THERMIQUE POUR UN ARRANGEMENT DE SURFACES COPLANAIRES DISPOSEES COMME DES TUILES ET ORIENTEES FRONTALEMENT VERS UN ECOULEMENT FORCE

Résumé—Des mesures de coefficient de transfert par tuile sont faites pour un arrangement de surfaces coplanaires disposées comme des tuiles et qui font face à un écoulement incident. L'écoulement balaie les tuiles en passant dans les fentes entre elles. Les expériences portent sur quatre configurations différentes caractérisées par le rapport de la largeur de la fente à la longueur de la tuile, et le nombre de Reynolds relatif à la fente varie de plus d'un orde de grandeur. Des expériences auxilaires concernent la visualisation et la variation du nombre de fentes pour démonter que les résultats ne sont pas influencés par les effets d'extrémité et par le nombre fini de tuiles enployées. On trouve que la dépendance du nombre de Nusselt sur le nombre de Reynolds est la même pour toutes les configurations étudiées et que l'influence de la géométrie de l'arrangement est bien représentée par une loi puissance. Cela conduit à une formule globale $Nu_p = 1{,}19\ Re^{0{,}465}\ Pr^{0{,}375}\ (P/W)^{1/4}$ pour laquelle l'écart-type avec les résultats expérimentaux est seulement de 1,1%.

WÄRMEÜBERGANG AN EINEM FELD PARALLEL ORIENTIERTER STREIFENFÖRMIGER OBERFLÄCHEN MIT SENKRECHTER ANSTRÖMUNG BEI ERZWUNGENER KONVEKTION

Zusammenfassung—Es wurden Messungen zur Bestimmung des Wärmeübergangskoeffizienten in einem Feld von parallel orientierten streifenförmigen Oberflächen gemacht, die normal zu einer ankommenden Strömung stehen. Die Strömung fließt zunächst über die Streifen und dann durch Zwischenräume, die von den Streifen gebildet werden. Die Versuche wurden für vier verschiedene Streifen-Spalt-Anordnungen durchgeführt. Dabei wurde das Verhältnis von Spalt-zu Streifenbreite variiert, wobei sich die Reynolds-Zahl, bezogen auf den Spalt, um mehr als eine Größenordnung änderte. Weitere Experimente wurden gemacht, um die Strömung sichtbar zu machen und zu zeigen, daß bei einer Vergrößerung der Anzahl der Spalte keine Veränderung des Ergebnisses durch Randeinflüsse gegenüber der untersuchten Anzahl eintritt. Es stellte sich heraus, daß die Abhängigkeit der Nusselt-Zahl von der Reynolds-Zahl für alle Anordnungskonfigurationen gleich war und daß der Einfluß der Anordnungsgeometrie sehr gut durch ein Potenzgesetz wiedergegeben werden konnte. Mit der allgemeinen Beziehung

$$Nu_p = 1{,}19\ Re^{0{,}465}\ Pr^{0{,}375}\ (P/W)^{1/4}$$

lassen sich die Ergebnisse mit einem mittleren quadratischen Fehler von nur 1,1% korrelieren.

ТЕПЛОПЕРЕНОС НА ПОВЕРХНОСТИ НАБОРА ПОПЕРЕЧНО ОБТЕКАЕМЫХ РАСПОЛОЖЕННЫХ В ОДНОЙ ПЛОСКОСТИ ПЛАНОК ПРИ ВЫНУЖДЕННОЙ КОНВЕКЦИИ

Аннотация—Для набора расположенных в одной плоскости планок, обращенных исследуемой поверхностью к набегающему потоку, измерены коэффициенты теплообмена каждой планки. Поток обтекает планки при входе в щелевидные зазоры между ними. Эксперименты проводились для четырех различных комбинаций планок и щелей, характеризующихся отношением ширины щели к ширине планки, причем значения числа Рейнольдса для щели изменялось более чем на порядок величины. Были проведены дополнительные эксперименты по визуализации потока с различным числом щелей для подтверждения того факта, что результаты экспериментов не зависят от концевых эффектов и конечного числа щелей. Показано, что зависимость числа Нуссельта от числа Рейнольдса остается одинаковой для всех комбинаций и что влияние геометрии системы хорошо описывается степенным законом. Это позволило предложить следующее обобщенное расчетное соотношение

$$Nu_P = 1{,}19\,Re^{0{,}465}\,Pr^{0{,}375}\,(P/W)^{1/4}.$$

При его использовании среднеквадратичная погрешность не превышает 1,1%.